

High Order Theory Approach for Debonded Sandwich Panels

Part I: Formulation and Displacement Fields

Zhangxian Yuan¹ and George A. Kardomateas²

Abstract

A high-order theory is developed to model asymmetric sandwich panels with face/core debonds and to provide a solution for the energy release rate and mode mixity. This new theory is a novel re-formulation of the Extended High-order Sandwich Panel theory (EHSAPT), in which faces and core were originally considered to be perfectly bonded. In the new formulation, a sandwich panel with an interfacial debond can be divided into three parts, namely, the debonded part, the substrate part, and the base part. A new high order displacement pattern is developed to describe the core's deformation in the substrate part, and it is compatible with the displacement field of the core in the base part. In addition capturing the high order shear deformation of the core, this new theory is able to take the transverse compressibility and axial rigidity of the core into account. In this Part I of this two-part research we focus on the formulation and the displacement field. In Part II, the fracture parameters, namely the energy release rate and the mode mixity will be addressed. Accordingly, in this paper, results for the deformation of the debonded panel are produced and compared with the ones given by the finite element method with a very fine mesh. The accuracy is proven for a wide range of core materials and for a wide range of debond lengths.

1. Introduction

A typical sandwich panel has two stiff thin face sheets bonded to a soft low density

¹Aerospace Engineering Department, Worcester Polytechnic Institute, Worcester, MA, 01609-2280, USA

²School of Aerospace Engineering, Georgia Institute of Technology, Atlanta, GA, 30332-0150, USA

core. Benefiting from this configuration, sandwich composite structures are highly efficient structures that exhibit high stiffness and strength with low resultant weight. They are widely used in the aerospace, marine, ground transportation, civil construction, and many other industries. In these sandwich structures, the interface between the faces and core is justifiably considered to be the weak link. Interfacial debonding between the faces and core is one of the most common failure modes of sandwich structures. It may occur due to manufacturing defects, impact or fatigue loading, etc. Such interfacial debonds will degrade the structural integrity and reduce the load carrying capacity and they may even cause catastrophic failure. Therefore, it is of great importance to be able to have an analytical model for sandwich structures with interfacial debonds, from which fracture quantities such as the energy release rate and the mode mixity can be accurately determined, in order to design reliable sandwich composite structures.

One feature of the modern sandwich structures is the usage of soft core materials, which results into a significant shear effect on the structural behavior [1]. The earliest models of sandwich analysis are the classical or first order shear models, which are based on the Euler-Bernoulli or Timoshenko beam theories. For the perfectly bonded sandwich structures made with very soft core under quasi-static loading, these models have been shown to be inaccurate in predicting displacements [2,3]. This implies that a high order shear deformation should be considered when modelling the interfacial debonding of sandwich structures. Several high order sandwich theories were developed to model the prefectly bonded sandwich structures, e.g, High-order Sandwich Panel Theory (HSAPT) [4], Extended High-order Sandwich Panel Theory (EHSAPT) [2], etc. Among these high order theories, the EHSAPT is the only theory that can account for the axial, transverse, and shear rigidity of the core. The high

order shear deformation of the core is embedded in the EHSAPT. It shows high accuracy and yields almost identical displacements and stresses to the elasticity for both static behavior [2] and dynamic response [5,6]. The EHSAPT has also been successfully applied to investigate the stability [7-10] and geometric nonlinearity effects on sandwich panels [9-11]. However, these studies are all limited to the perfectly bonded sandwich structures.

The main objective of this paper is to present a robust and self-contained approach to model sandwich panels with face/core interfacial debonds and to evaluate the corresponding fracture parameters. This will be reported in a two-part series of papers. In this Part I, first we develop a new high order analytical model for debonded sandwich structures based on the EHSAPT (the latter was developed for perfectly bonded sandwich panels only). New displacement field assumptions are proposed to describe the deformation of the debonded part and the substrate part. The formulation incorporates the core's high order shear deformation, the core's axial rigidity, and the core's transverse compressibility. It is applicable to sandwich panels made with a wide range of core materials, including very soft ones. By introducing equivalent resultant forces and moments, the governing equations are obtained as a set of first order differential equations. In Part II, these displacement field solutions will be used to obtain closed form expressions for the energy release and the mode mixity. Solutions from this theory will be compared with the corresponding displacements from finite element analyses. Results will be obtained for a wide range of material combinations and for sandwich panels with different debond lengths.

2. Formulation of sandwich panels with an interfacial debond

A sandwich panel with a face/core interfacial debond is schematically shown in Fig. 1a. The length of the debond is a , and the length of the bonded part is L . Therefore, the total

length of the sandwich beam is $L + a$. The thickness of the top face, core, and bottom face are f_t , f_b , and $2c$, respectively. A right-hand Cartesian coordinate system is set with the origin placed at the cross section of the crack tip. The x axis coincides with the middle line of the core, and the z axis is along the thickness direction and passes the crack tip. As a plane problem is considered, a unit width is considered for simplicity. To model a sandwich panel with a face/core debond, the sandwich panel is divided into three parts, as shown in Fig. 1b: the “debonded” part, the “substrate” part and the “base” part. Both the “debonded” (top face) and the “substrate” (below the debond) parts are over the length of the beam that contains the debond. The “base” part is the intact region of the beam.

It is seen that the base part is the same as a sandwich panel with perfectly bonded faces and core. Therefore, the Extended High-order Sandwich Panel Theory (EHSAPT) is employed in the base part directly. In the substrate part, a re-formulation of the theory is needed, since there is no top face/core continuity to be enforced. In this re-formulation, the displacement of the core is considered analogous to that of the base part, but it only includes the continuity condition at the bottom face/core interface. The debonded top face (debonded part) is modeled separately. In this way, the upper surface of the debond (the lower surface of the debonded part) and the lower surface of the debond (the upper surface of the core of the substrate part) are allowed to move freely. Additionally, the continuity conditions of the cross section at $x = 0$, which is the connected cross section of the base, substrate, and debonded parts, should be enforced. In the following, we use capital letters for the different parts, i.e., B (base part), S (substrate), D (debonded part) and we use lower case letters for the different layers, b (bottom face, c (core) and t (top face).

2.1 Displacement field

Part that I am
planning to validate

*As the deformation
is less*

2.1.1 Base part

In the base part, the deformation follows the Extended High-order Sandwich Panel theory [22]. The thin high stiffness top and bottom faces are modeled as two Euler-Bernoulli beams, and the core has a high order displacement pattern. In the core, the axial displacement and the transverse displacement are a cubic function of z and a quadratic function of z , respectively. The displacement field in the top face ($c < z \leq c + f_t$) is:

$$w^{Bt}(x, z) = w_0^{Bt}(x) ; \quad u^{Bt}(x, z) = u_0^{Bt}(x) - \left(z - c - \frac{f_t}{2} \right) w_{0,x}^{Bt}(x) , \quad (1a)$$

and in bottom face ($-c - f_b \leq z < -c$),

$$w^{Bb}(x, z) = w_0^{Bb}(x) ; \quad u^{Bb}(x, z) = u_0^{Bb}(x) - \left(z + c + \frac{f_b}{2} \right) w_{0,x}^{Bb}(x) , \quad (1b)$$

where $u_0^{Bt,Bb}$ and $w_0^{Bt,Bb}$ are the axial and transverse displacements of the centroid of the top and bottom faces, and the subscript comma x is the first order derivative with respect to x . The superscript B is added to denote the displacement field in the base part.

In the core, high order polynomials are used to describe the deformation, thus, the axial and transverse displacements are assumed in the form:

$$w^{Bc}(x, z) = w_0^{Bc}(x) + w_1^{Bc}(x)z + w_2^{Bc}(x)z^2 , \quad (2a)$$

$$u^{Bc}(x, z) = u_0^{Bc}(x) + \phi_0^{Bc}(x)z + u_2^{Bc}(x)z^2 + u_3^{Bc}(x)z^3 , \quad (2b)$$

where u_0^{Bc} and w_0^{Bc} are the axial and transverse displacements and ϕ_0^{Bc} is the slope of the centerline of the core.

Imposing the transverse displacement continuity condition at the face/core interfaces in

the base part, namely $w^{Bc}(x, c) = w^{Bt}(x, c)$ and $w^{Bc}(x, -c) = w^{Bb}(x, -c)$, we can solve for the $w_1^{Bc}(x)$ and $w_2^{Bc}(x)$, and thus derive the core transverse displacement in the base part:

$$w^{Bc}(x, z) = \left(\frac{z}{2c} + \frac{z^2}{2c^2} \right) w_0^{Bt}(x) + \left(1 - \frac{z^2}{c^2} \right) w_0^{Bc}(x) + \left(-\frac{z}{2c} + \frac{z^2}{2c^2} \right) w_0^{Bb}(x) . \quad (3a)$$

Similarity, $u_2^{Bc}(x)$ and $u_3^{Bc}(x)$ are determined from the axial displacement displacement continuity condition at the face/core interfaces, namely $u^{Bc}(x, c) = u^{Bt}(x, c)$ and $u^{Bc}(x, -c) = u^{Bb}(x, -c)$. Thus, Eq. (2b) becomes:

$$\begin{aligned} u^{Bc}(x, z) = & \frac{z^2}{2c^2} \left(1 + \frac{z}{c} \right) u_0^{Bt}(x) + \frac{f_t z^2}{4c^2} \left(1 + \frac{z}{c} \right) w_{0,x}^{Bt}(x) + \left(1 - \frac{z^2}{c^2} \right) u_0^{Bc}(x) + \\ & + z \left(1 - \frac{z^2}{c^2} \right) \phi_0^{Bc}(x) + \frac{z^2}{2c^2} \left(1 - \frac{z}{c} \right) u_0^{Bb}(x) + \frac{f_b z^2}{4c^2} \left(-1 + \frac{z}{c} \right) w_{0,x}^{Bb}(x) . \end{aligned} \quad (3b)$$

2.1.2 Substrate part

The substrate part only contains the core layer and the bottom face. Thus the theory needs to be re-formulated. We assume that the bottom face of the substrate part has the same displacement field as that in the base part, which is:

$$w^{Sb}(x, z) = w_0^{Sb}(x) . \quad (4a)$$

$$u^{Sb}(x, z) = u_0^{Sb}(x) - \left(z + c + \frac{f_b}{2} \right) w_{0,x}^{Sb}(x) . \quad (4b)$$

where the subscript S is added to denote the displacement field in the substrate part. w_0^{Sb} and u_0^{Sb} have the same definitions as the w_0^{Bb} and u_0^{Bb} ones in the base part.

In the substrate part, the bottom face and the core are perfectly bonded. Furthermore, core's deformation should be compatible to the deformation of the core belonging to the base

part. Thus, a novel high order displacement assumption is developed for the core belonging to the substrate part. It is given as:

$$w^{Sc}(x, z) = \left(\frac{z}{2c} + \frac{z^2}{2c^2} \right) w^{St}(x) + \left(1 - \frac{z^2}{c^2} \right) w_0^{Sc}(x) + \left(-\frac{z}{2c} + \frac{z^2}{2c^2} \right) w_0^{Sb}(x) , \quad (5a)$$

$$\begin{aligned} u^{Sc}(x, z) = & \frac{z^2}{2c^2} \left(1 + \frac{z}{c} \right) u^{St}(x) + \left(1 - \frac{z^2}{c^2} \right) u_0^{Sc}(x) + z \left(1 - \frac{z^2}{c^2} \right) \phi_0^{Sc}(x) + \\ & + \frac{z^2}{2c^2} \left(1 - \frac{z}{c} \right) u_0^{Sb}(x) + \frac{f_b z^2}{4c^2} \left(-1 + \frac{z}{c} \right) w_{0,x}^{Sb}(x) , \end{aligned} \quad (5b)$$

where $u^{St}(x)$ and $w^{St}(x)$ represent the axial and transverse displacements of the top edge of the core ($z = c, -a \leq x \leq 0$). These are the additional functions needed for the high order theory for the case of a debond. Notice that the superscript S stands for the substrate part. The displacement continuity conditions at the interface of the core and the bottom face ($z = -c$) can be easily verified.

Therefore, the displacement field of the substrate part is in terms of seven generalized coordinates, namely the $u^{St}(x)$, $w^{St}(x)$, $u_0^{Sc}(x)$, $w_0^{Sc}(x)$, $\phi_0^{Sc}(x)$, $u_0^{Sb}(x)$ and $w_0^{Sb}(x)$, which are functions of x coordinate.

At the cross section between the substrate part and the base part (cross section at $x = 0$), in addition to the continuity of displacements in the core and bottom face, which mean that:

$$\begin{aligned} w_0^{Sc}(0) &= w_0^{Bc}(0) ; \quad u_0^{Sc}(0) = u_0^{Bc}(0) ; \quad w_0^{Sb}(0) = w_0^{Bb}(0) ; \quad u_0^{Sb}(0) = u_0^{Bb}(0) ; \\ w_{0,x}^{Sb}(0) &= w_{0,x}^{Bb}(0) ; \quad \phi_0^{Sc}(0) = \phi_0^{Bc}(0) , \end{aligned} \quad (6)$$

two more conditions need be satisfied, namely equality of the axial and transverse displacements at the top of the substrate, $z = c$, from Eqn (5a,b) and (3a,b):

$$u^{St}(0) = u_0^{Bt}(0) + \frac{f_t}{2} w_{0,x}^{Bt}(0) , \quad (7a)$$

$$w^{St}(0) = w_0^{Bt}(0) , \quad (7b)$$

which are the axial and transverse displacement continuity condition of the crack tip ($x = 0$, $z = c$) between the substrate part and the base part.

2.1.3 Debonded part

The debonded part only contains the thin high stiffness face sheet, and is modeled as an Euler-Bernoulli beam, which gives:

$$w^{Dt}(x, z) = w_0^{Dt}(x) , \quad (8a)$$

$$u^{Dt}(x, z) = u_0^{Dt}(x) - \left(z - c - \frac{f_t}{2} \right) w_{0,x}^{Dt}(x) , \quad (8b)$$

where the superscript D stands for the debonded part and $u_0^{Dt}(x)$ and $w_0^{Dt}(x)$ have the same meaning as the $u_0^{Bt}(x)$ and $w_0^{Bt}(x)$ in the base part.

2.2 Kinematic and constitutive relations

The strains are obtained from the displacements using the linear strain-displacement relations, i.e., for $k = Bt, Bc, Bb, Sc, Sb, Dt$:

$$\epsilon_{xx}^k(x, z) = u_{,x}^k(x, z) ; \quad \epsilon_{zz}^k(x, z) = w_{,z}^k(x, z) ; \quad \gamma_{xz}^k(x, z) = u_{,z}^k(x, z) + w_{,x}^k(x, z) . \quad (9a)$$

For simplicity of presentation, the (x, z) will be neglected in the functions. Same simplifications are applied with respect to the (x) and (z) dependencies.

As the Euler-Bernoulli assumptions are adopted in the faces, the axial normal strain is the only non-zero strain. So, the axial normal stress of the faces are,

$$\sigma_{xx}^i = E_1^t \epsilon_{xx}^i \quad (i = Bt, Dt) ; \quad \sigma_{xx}^j = E_1^b \epsilon_{xx}^j \quad (j = Bb, Sb) . \quad (9b)$$

In the core, the axial normal stress σ_{xx}^k , transverse normal stress σ_{zz}^k , and the shear stress τ_{xz}^k are

$$\begin{bmatrix} \sigma_{xx}^k \\ \sigma_{zz}^k \\ \tau_{xz}^k \end{bmatrix} = \begin{bmatrix} C_{11}^c & C_{13}^c & 0 \\ C_{13}^c & C_{33}^c & 0 \\ 0 & 0 & C_{55}^c \end{bmatrix} \begin{bmatrix} \epsilon_{xx}^k \\ \epsilon_{zz}^k \\ \gamma_{xz}^k \end{bmatrix}, \quad (k = Bc, Sc) \quad (9c)$$

When orthotropic material is used to construct the core, $[C^c]$ is given by the inverse of the compliance matrix, namely

$$\begin{bmatrix} C_{11}^c & C_{13}^c & 0 \\ C_{13}^c & C_{33}^c & 0 \\ 0 & 0 & C_{55}^c \end{bmatrix} = \begin{bmatrix} \frac{1}{E_1^c} & -\frac{\nu_{31}^c}{E_3^c} & 0 \\ -\frac{\nu_{31}^c}{E_3^c} & \frac{1}{E_3^c} & 0 \\ 0 & 0 & \frac{1}{G_{31}^c} \end{bmatrix}^{-1}. \quad (9d)$$

2.3 Principle of minimum potential energy

The governing equations are derived from the principle of minimum potential energy,

$$\delta\Pi = \delta(U_{base} + U_{substrate} + U_{debonded} + V) = 0. \quad (10a)$$

where U_{base} , $U_{substrate}$, and $U_{debonded}$ are the strain energies of the base part, the substrate part, and the debonded part, respectively,

$$\begin{aligned} \delta U_{base} = & \int_0^L \left[\int_c^{c+f_t} \sigma_{xx}^{Bt} \delta \epsilon_{xx}^{Bt} dz + \int_{-c}^c (\sigma_{xx}^{Bc} \delta \epsilon_{xx}^{Bc} + \sigma_{zz}^{Bc} \delta \epsilon_{zz}^{Bc} + \tau_{xz}^{Bc} \delta \gamma_{xz}^{Bc}) dz + \right. \\ & \left. + \int_{-c-f_b}^{-c} \sigma_{xx}^{Bb} \delta \epsilon_{xx}^{Bb} dz \right] dx. \end{aligned} \quad (10b)$$

$$\delta U_{substrate} = \int_{-a}^0 \left[\int_{-c}^c (\sigma_{xx}^{Sc} \delta \epsilon_{xx}^{Sc} + \sigma_{zz}^{Sc} \delta \epsilon_{zz}^{Sc} + \tau_{xz}^{Sc} \delta \gamma_{xz}^{Sc}) dz + \int_{-c-f_b}^{-c} \sigma_{xx}^{Sb} \delta \epsilon_{xx}^{Sb} dz \right] dx. \quad (10c)$$

$$\delta U_{debonded} = \int_{-a}^0 \int_c^{c+f_t} \sigma_{xx}^{Dt} \delta \epsilon_{xx}^{Dt} dz dx. \quad (10d)$$

With the sign convention shown in Fig. 2, the external potential energy, V , is given by

$$\begin{aligned}\delta V = & - \int_{-a}^L (p^t \delta u_0^t + p^b \delta u_0^b + q^t \delta w_0^t + q^b \delta w_0^b - m^t \delta w_{0,x}^t - m^b \delta w_{0,x}^b) dx - \\ & - \tilde{N}^t \delta u_0^t \Big|_{x=-a}^{x=L} - \tilde{N}^b \delta u_0^b \Big|_{x=-a}^{x=L} - \tilde{N}^c \delta u_0^c \Big|_{x=-a}^{x=L} - \\ & - \tilde{V}^t \delta w_0^t \Big|_{x=-a}^{x=L} - \tilde{V}^b \delta w_0^b \Big|_{x=-a}^{x=L} - \tilde{V}^c \delta w_0^c \Big|_{x=-a}^{x=L} + \\ & + \tilde{M}^t \delta w_{0,x}^t \Big|_{x=-a}^{x=L} + \tilde{M}^b \delta w_{0,x}^b \Big|_{x=-a}^{x=L} + \tilde{M}^c \delta \phi_0^c \Big|_{x=-a}^{x=L} .\end{aligned}\quad (10e)$$

with

$$\begin{aligned}[u_0^t, w_0^t] = & \begin{cases} [u_0^{Dt}, w_0^{Dt}] & (-a \leq x < 0) \\ [u_0^{Bt}, w_0^{Bt}] & (0 \leq x \leq L) \end{cases}; \quad [u_0^b, w_0^b] = \begin{cases} [u_0^{Sb}, w_0^{Sb}] & (-a \leq x < 0) \\ [u_0^{Bb}, w_0^{Bb}] & (0 \leq x \leq L) \end{cases}; \\ [u_0^c, w_0^c, \phi_0^c] = & \begin{cases} [u_0^{Sc}, w_0^{Sc}, \phi_0^{Sc}] & (-a \leq x < 0) \\ [u_0^{Bc}, w_0^{Bc}, \phi_0^{Bc}] & (0 \leq x \leq L) \end{cases}.\end{aligned}\quad (10f)$$

where $\tilde{p}^{t,b}$ and $\tilde{q}^{t,b}$ are distributed loads along axial and transverse directions, $\tilde{m}^{t,b}$ are the distributed moment, $\tilde{N}^{t,b,c}$ are the axial concentrated loads acting on edges, $\tilde{V}^{t,b,c}$ are the edge shear forces, and $\tilde{M}^{t,b,c}$ are the moment at the edge.

2.3.1 Governing equations of the base part

The variational principle of Eq. (10a) leads to three sets of equations, which describe the base part, and substrate part, and the debonded part, respectively. In order to achieve first order differential equations as the governing equations, stress resultants and equivalent resultant forces are introduced. The base part is considered first to illustrate the derivation procedures. Before listing the equations, stress resultants and couples of three layers are defined first, which are,

$$N_x^{Bt} = \int_c^{c+f_t} \sigma_{xx}^{Bt} dz = C_{11}^t f_t u_{0,x}^{Bt}; \quad N_x^{Bb} = \int_{-c-f_b}^{-c} \sigma_{xx}^{Bb} dz = C_{11}^b f_b u_{0,x}^{Bb}, \quad (11a)$$

$$N_x^{Bc} = \int_{-c}^c \sigma_{xx}^{Bc} dz = C_{13}^c (w_0^{Bt} - w_0^{Bb}) + \frac{cC_{11}^c}{3} \left(u_{0,x}^{Bt} + 4u_{0,x}^{Bc} + u_{0,x}^{Bb} + \frac{f_t}{2} w_{0,xx}^{Bt} - \frac{f_b}{2} w_{0,xx}^{Bb} \right) , \quad (11b)$$

$$M_y^{Bt} = \int_c^{c+f_t} \sigma_{xx}^{Bt} \left(z - c - \frac{f_t}{2} \right) dz = -C_{11}^t \frac{f_t^3}{12} w_{0,xx}^{Bt} , \quad (11c)$$

$$M_y^{Bb} = \int_{-c-f_b}^{-c} \sigma_{xx}^{Bb} \left(z + c + \frac{f_b}{2} \right) dz = -C_{11}^b \frac{f_b^3}{12} w_{0,xx}^{Bb} , \quad (11d)$$

$$\begin{aligned} M_y^{Bc} &= \int_{-c}^c \sigma_{xx}^{Bc} z dz = \frac{2cC_{13}^c}{3} (w_0^{Bt} - 2w_0^{Bc} + w_0^{Bb}) + \\ &+ \frac{c^2 C_{11}^c}{30} [6(u_{0,x}^{Bt} - u_{0,x}^{Bb}) + 8c\phi_{0,x}^{Bc} + 3(f_t w_{0,xx}^{Bt} + f_b w_{0,xx}^{Bb})] , \end{aligned} \quad (11e)$$

$$Q_{xz}^{Bc} = \int_{-c}^c \tau_{xz}^{Bc} dz = C_{55}^c \left[(u_0^{Bt} - u_0^{Bb}) + \left(\frac{c}{3} + \frac{f_t}{2} \right) w_{0,x}^{Bt} + \left(\frac{c}{3} + \frac{f_b}{2} \right) w_{0,x}^{Bb} + \frac{4}{3} c w_{0,x}^{Bc} \right] . \quad (11f)$$

Additionally, due to the high order displacement pattern in the core, high order stress resultants are also defined, which are,

$$[M_{xx2}^{Bc}, M_{xx3}^{Bc}] = \int_{-c}^c [z^2, z^3] \sigma_{xx}^{Bc} dz , \quad (12a)$$

$$[M_{xz1}^{Bc}, M_{xz2}^{Bc}] = \int_{-c}^c [z, z^2] \tau_{xz}^{Bc} dz , \quad (12b)$$

$$[M_{zz0}^{Bc}, M_{zz1}^{Bc}] = \int_{-c}^c [1, z] \sigma_{zz}^{Bc} dz . \quad (12c)$$

Similar to the stress resultants and couples given by Eq. (11), high order stress resultants,

M_{xx2}^{Bc} , M_{xx3}^{Bc} , M_{xz1}^{Bc} , M_{xz2}^{Bc} , M_{zz0}^{Bc} , and M_{zz1}^{Bc} , contain terms of $u_{0,x}^{Bt}$, $u_{0,x}^{Bb}$, $u_{0,x}^{Bc}$, $w_{0,xx}^{Bt}$, $w_{0,xx}^{Bb}$, $w_{0,x}^{Bc}$, $\phi_{0,x}^{Bc}$, and terms of u_0^{Bt} , u_0^{Bb} , u_0^{Bc} , $w_{0,x}^{Bt}$, $w_{0,x}^{Bb}$, and ϕ_0^{Bc} .

Then, the variational principle of Eq. (13) leads to the following 9 equations for the base part ($0 \leq x \leq L$),

$$\frac{d\bar{N}^{Bt}}{dx} = \frac{1}{c^2} M_{xz1}^{Bc} + \frac{3}{2c^3} M_{xz2}^{Bc} - p^t , \quad (13a)$$

$$\frac{d\bar{N}^{Bb}}{dx} = \frac{1}{c^2} M_{xz1}^{Bc} - \frac{3}{2c^3} M_{xz2}^{Bc} - p^b , \quad (13b)$$

$$\frac{d\bar{N}^{Bc}}{dx} = -\frac{2}{c^2} M_{xz1}^{Bc} . \quad (13c)$$

$$\frac{d\bar{M}^{Bt}}{dx} = \bar{V}^{Bt} - \left(\frac{1}{2c} + \frac{f_t}{2c^2} \right) M_{xz1}^{Bc} - \left(\frac{1}{2c^2} + \frac{3f_t}{4c^3} \right) M_{xz2}^{Bc} - m^t , \quad (13d)$$

$$\frac{d\bar{V}^{Bt}}{dx} = \frac{1}{2c} M_{zz0}^{Bc} + \frac{1}{c^2} M_{zz1}^{Bc} - q^t , \quad (13e)$$

$$\frac{d\bar{M}^{Bb}}{dx} = \bar{V}^{Bb} + \left(\frac{1}{2c} + \frac{f_b}{2c^2} \right) M_{xz1}^{Bc} - \left(\frac{1}{2c^2} + \frac{3f_b}{4c^3} \right) M_{xz2}^{Bc} - m^b , \quad (13f)$$

$$\frac{d\bar{V}^{Bb}}{dx} = -\frac{1}{2c} M_{zz0}^c + \frac{1}{c^2} M_{zz1}^c - q^b , \quad (13g)$$

$$\frac{d\bar{M}^{Bc}}{dx} = Q_{xz}^{Bc} - \frac{3}{c^2} M_{xz2}^{Bc} , \quad (13h)$$

$$\frac{d\bar{V}^{Bc}}{dx} = -\frac{2}{c^2} M_{zz1}^{Bc} . \quad (13i)$$

where $\bar{N}^{Bt, Bb, Bc}$, $\bar{M}^{Bt, Bb, Bc}$, $\bar{V}^{Bt, Bb, Bc}$ are the equivalent resultant forces in the base part (B), and are defined by,

$$\bar{N}^{Bt} = N_x^{Bt} + \frac{1}{2c^2} M_{xx2}^{Bc} + \frac{1}{2c^3} M_{xx3}^{Bc} , \quad (14a)$$

$$\bar{N}^{Bb} = N_x^{Bb} + \frac{1}{2c^2} M_{xx2}^{Bc} - \frac{1}{2c^3} M_{xx3}^{Bc} , \quad (14b)$$

$$\bar{N}^{Bc} = N_x^{Bc} - \frac{1}{c^2} M_{xx2}^{Bc} , \quad (14c)$$

$$\bar{M}^{Bt} = M_y^{Bt} - \frac{f_t}{4c^2} M_{xx2}^{Bc} - \frac{f_t}{4c^3} M_{xx3}^{Bc} , \quad (14d)$$

$$\bar{M}^{Bb} = M_y^{Bb} + \frac{f_b}{4c^2} M_{xx2}^{Bc} - \frac{f_b}{4c^3} M_{xx3}^{Bc} , \quad (14e)$$

$$\bar{M}^{Bc} = M_y^{Bc} - \frac{1}{c^2} M_{xx3}^{Bc} , \quad (14f)$$

$$\bar{V}^{Bc} = Q_{xz}^{Bc} - \frac{1}{c^2} M_{xz2}^{Bc} . \quad (14g)$$

After substituting Eq. (11) and Eq. (12) into Eq. (14), the right hand side of Eq. (14) only contains terms of $u_{0,x}^{Bt}$, $u_{0,x}^{Bb}$, $u_{0,x}^{Bc}$, $w_{0,xx}^{Bt}$, $w_{0,xx}^{Bb}$, $w_{0,x}^{Bc}$, $\phi_{0,x}^{Bc}$, and terms of u_0^{Bt} ,

u_0^{Bb} , u_0^{Bc} , $w_{0,x}^{Bt}$, $w_{0,x}^{Bb}$, and ϕ_0^{Bc} . Therefore, 7 higher order displacement unknowns, namely $u_{0,x}^{Bt}$, $u_{0,x}^{Bb}$, $u_{0,x}^{Bc}$, $w_{0,xx}^{Bt}$, $w_{0,xx}^{Bb}$, $\phi_{0,x}^{Bc}$, and $w_{0,x}^{Bc}$, are solved in terms of the equivalent resultant forces, $\bar{N}^{Bt,Bb,Bc}$, $\bar{M}^{Bt,Bb,Bc}$, \bar{V}^{Bc} , and the lower order displacement unknowns, $u_0^{Bt,Bb,Bc}$, $w_0^{Bt,Bb,Bc}$, $w_{0,x}^{Bt,Bb}$, ϕ_0^{Bc} . In other words, 7 first order differential equations are given as,

$$\frac{du_0^{Bt}}{dx} = f^{B1}(\mathbf{u}^B, \bar{\mathbf{N}}^B) ; \quad \frac{du_0^{Bb}}{dx} = f^{B2}(\mathbf{u}^B, \bar{\mathbf{N}}^B) ; \quad \frac{du_0^{Bc}}{dx} = f^{B3}(\mathbf{u}^B, \bar{\mathbf{N}}^B) , \quad (15a)$$

$$\frac{dw_{0,x}^{Bt}}{dx} = f^{B4}(\mathbf{u}^B, \bar{\mathbf{N}}^B) ; \quad \frac{dw_{0,x}^{Bb}}{dx} = f^{B5}(\mathbf{u}^B, \bar{\mathbf{N}}^B) ; \quad \frac{dw_{0,x}^{Bc}}{dx} = f^{B6}(\mathbf{u}^B, \bar{\mathbf{N}}^B) , \quad (15b)$$

$$\frac{d\phi_0^{Bc}}{dx} = f^{B7}(\mathbf{u}^B, \bar{\mathbf{N}}^B) . \quad (15c)$$

where $f^{Bj}(\mathbf{u}^B, \bar{\mathbf{N}}^B)$ ($j = 1, \dots, 7$) stand for the expressions after solving the 7 higher order displacements from Eq. (14). These expressions are in terms of displacement unknowns $\mathbf{u}^B = \{u_0^{Bt}, u_0^{Bb}, u_0^{Bc}, w_0^{Bt}, w_0^{Bb}, w_0^{Bc}, w_{0,x}^{Bt}, w_{0,x}^{Bb}, \phi_0^{Bc}\}$, and equivalent resultant force unknowns $\bar{\mathbf{N}}^B = \{\bar{N}^{Bt}, \bar{N}^{Bb}, \bar{N}^{Bc}, \bar{M}^{Bt}, \bar{M}^{Bb}, \bar{M}^{Bc}, \bar{V}^{Bt}, \bar{V}^{Bb}, \bar{V}^{Bc}\}$. The detailed expressions are long and thus are omitted for conciseness.

After Substituting Eqs. (11), (12), and (15) into Eq. (13), the right-hand side of Eq. (13) only contains terms related to the equivalent resultant forces, $\bar{N}^{t,b,c}$, $\bar{M}^{t,b,c}$, $\bar{V}^{t,b,c}$, and the lower order displacement unknowns, $u_0^{t,b,c}$, $w_0^{t,b,c}$, $w_{0,x}^{t,b}$, ϕ_0^c . These equations can be written as,

$$\frac{d\bar{N}^{Bt}}{dx} = f^{B8}(\mathbf{u}^B, \bar{\mathbf{N}}^B) ; \quad \frac{d\bar{N}^{Bb}}{dx} = f^{B9}(\mathbf{u}^B, \bar{\mathbf{N}}^B) ; \quad \frac{d\bar{N}^{Bc}}{dx} = f^{B10}(\mathbf{u}^B, \bar{\mathbf{N}}^B) ; , \quad (16a)$$

$$\frac{d\bar{M}^{Bt}}{dx} = f^{B11}(\mathbf{u}^B, \bar{\mathbf{N}}^B) ; \quad \frac{d\bar{M}^{Bb}}{dx} = f^{B12}(\mathbf{u}^B, \bar{\mathbf{N}}^B) ; \quad \frac{d\bar{M}^{Bc}}{dx} = f^{B13}(\mathbf{u}^B, \bar{\mathbf{N}}^B) ; , \quad (16b)$$

$$\frac{d\bar{V}^{Bt}}{dx} = f^{B14}(\mathbf{u}^B, \bar{\mathbf{N}}^B) ; \quad \frac{d\bar{V}^{Bb}}{dx} = f^{B15}(\mathbf{u}^B, \bar{\mathbf{N}}^B) ; \quad \frac{d\bar{V}^{Bc}}{dx} = f^{B16}(\mathbf{u}^B, \bar{\mathbf{N}}^B) ; . \quad (16c)$$

where $f^{Bj}(\mathbf{u}^B, \bar{\mathbf{N}}^B)$ ($j = 8, \dots, 16$) stand for the final expressions of the right-hand side, and

are linear algebraic expressions in terms of $\mathbf{u}^B = \{u_0^{Bt}, u_0^{Bb}, u_0^{Bc}, w_0^{Bt}, w_0^{Bb}, w_0^{Bc}, w_{0,x}^{Bt}, w_{0,x}^{Bb}, \phi_0^{Bc}\}$ and $\bar{\mathbf{N}}^B = \{\bar{N}^{Bt}, \bar{N}^{Bb}, \bar{N}^{Bc}, \bar{M}^{Bt}, \bar{M}^{Bb}, \bar{M}^{Bc}, \bar{V}^{Bt}, \bar{V}^{Bb}, \bar{V}^{Bc}\}$. These detailed expressions are long and thus are omitted for conciseness.

Two more differential equations come from the relation between $w_{0,x}^{Bt,Bb}$ and $w_{0,xx}^{Bt,Bb}$, which are

$$\frac{dw_0^{Bt}}{dx} = w_{0,x}^{Bt} ; \quad \frac{dw_0^{Bb}}{dx} = w_{0,x}^{Bb} . \quad (17)$$

Therefore, Eqs. (15)-(17) give the governing equations of the base part, which contain 18 first order differential equations with 18 unknowns; 9 of the unknowns are the equivalent resultant forces, $\bar{N}^{Bt,Bb,Bc}$, $\bar{M}^{Bt,Bb,Bc}$, $\bar{V}^{Bt,Bb,Bc}$, and other 9 unknowns are the displacements and first order derivative of transverse displacement of faces, $u_0^{Bt,Bb,Bc}$, $w_0^{Bt,Bb,Bc}$, $w_{0,x}^{Bt,Bb}$, ϕ_0^{Bc} .

2.3.2 Governing equations of the substrate part

In the substrate part, the stress resultant forces and couples are defined first.

$$[N_x^{Sc}, M_y^{Sc}, M_{xx2}^{Sc}, M_{xx3}^{Sc}] = \int_{-c}^c [1, z, z^2, z^3] \sigma_{xx}^{Sc} dz , \quad (18a)$$

$$[Q_{xz}^{Sc}, M_{xz1}^{Sc}, M_{xz2}^{Sc}] = \int_{-c}^c [1, z, z^2] \tau_{xz}^{Sc} dz , \quad (18b)$$

$$[M_{zz0}^{Sc}, M_{zz1}^{Sc}] = \int_{-c}^c [1, z] \sigma_{zz}^{Sc} dz , \quad (18c)$$

$$[N_x^{Sb}, M_y^{Sb}] = \int_{-c-f_b}^{-c} \left[1, \left(z + c + \frac{f_b}{2} \right) \right] \sigma_{xx}^{Sb} dz . \quad (18d)$$

where the superscript S stands for terms defined in the substrate part, and stresses appeared in Eq. (18) come from Eq. (9) with Eqs. (6)-(7).

The variation of the total potential energy, Eq. (13), leads to another 8 equations corresponding to the substrate part ($-a \leq x \leq 0$).

$$\frac{d\bar{N}^{St}}{dx} = \frac{1}{c^2} M_{xz1}^{Sc} + \frac{3}{2c^3} M_{xz2}^{Sc} - p^t , \quad (19a)$$

$$\frac{d\bar{N}^{Sb}}{dx} = \frac{1}{c^2} M_{xz1}^{Sc} - \frac{3}{2c^3} M_{xz2}^{Sc} - p^b , \quad (19b)$$

$$\frac{d\bar{N}^{Sc}}{dx} = -\frac{2}{c^2} M_{xz1}^{Sc} , \quad (19c)$$

$$\frac{d\bar{V}^{St}}{dx} = \frac{1}{2c} M_{zz0}^{Sc} + \frac{1}{c^2} M_{zz1}^{Sc} - q^t , \quad (19d)$$

$$\frac{d\bar{M}^{Sb}}{dx} = \bar{V}^{Sb} + \left(\frac{1}{2c} + \frac{f_b}{2c^2} \right) M_{xz1}^{Sc} - \left(\frac{1}{2c^2} + \frac{3f_b}{4c^3} \right) M_{xz2}^{Sc} - m^b , \quad (19e)$$

$$\frac{d\bar{V}^{Sb}}{dx} = -\frac{1}{2c} M_{zz0}^{Sc} + \frac{1}{c^2} M_{zz1}^{Sc} - q^b , \quad (19f)$$

$$\frac{d\bar{M}^{Sc}}{dx} = Q_{xz}^{Sc} - \frac{3}{c^2} M_{xz2}^{Sc} , \quad (19g)$$

$$\frac{d\bar{V}^{Sc}}{dx} = -\frac{2}{c^2} M_{zz1}^{Sc} , \quad (19h)$$

where $\bar{N}^{St,Sb,Sc}$, $\bar{M}^{Sb,Sc}$, $\bar{V}^{St,Sb,Sc}$ are the equivalent resultant forces in the substrate part, and are defined by,

$$\bar{N}^{St} = \frac{1}{2c^2} M_{xx2}^{Sc} + \frac{1}{2c^3} M_{xx3}^{Sc} , \quad (20a)$$

$$\bar{N}^{Sb} = N_x^{Sb} + \frac{1}{2c^2} M_{xx2}^{Sc} - \frac{1}{2c^3} M_{xx3}^{Sc} , \quad (20b)$$

$$\bar{N}^{Sc} = N_x^{Sc} - \frac{1}{c^2} M_{xx2}^{Sc} , \quad (20c)$$

$$\bar{M}^{Sb} = M_y^{Sb} + \frac{f_b}{4c^2} M_{xx2}^{Sc} - \frac{f_b}{4c^3} M_{xx3}^{Sc} , \quad (20d)$$

$$\bar{M}^{Sc} = M_y^{Sc} - \frac{1}{c^2} M_{xx3}^{Sc}, \quad (20e)$$

$$\bar{V}^{Sc} = Q_{xz}^{Sc} - \frac{1}{c^2} M_{xz2}^{Sc}, \quad (20f)$$

$$\bar{V}^{St} = \frac{1}{2c} M_{xz1}^{Sc} + \frac{1}{2c^2} M_{xz2}^{Sc}. \quad (20g)$$

Analogous to the base part, 7 higher order displacements, namely $u_{,x}^{St}$, $w_{,x}^{St}$, $u_{0,x}^{Sb}$, $u_{0,x}^{Sc}$,

$w_{0,xx}^{Sb}$, $\phi_{0,x}^{Sc}$, and $w_{0,x}^{Sc}$, are solved from Eq. (20). It can be written as,

$$\frac{du^{St}}{dx} = f^{S1}(\mathbf{u}^S, \bar{\mathbf{N}}^S); \quad \frac{du_0^{Sb}}{dx} = f^{S2}(\mathbf{u}^S, \bar{\mathbf{N}}^S); \quad \frac{du_0^{Sc}}{dx} = f^{S3}(\mathbf{u}^S, \bar{\mathbf{N}}^S), \quad (21a)$$

$$\frac{dw^{St}}{dx} = f^{S4}(\mathbf{u}^S, \bar{\mathbf{N}}^S); \quad \frac{dw_{0,x}^{Sb}}{dx} = f^{S5}(\mathbf{u}^S, \bar{\mathbf{N}}^S); \quad \frac{dw_0^{Sc}}{dx} = f^{S6}(\mathbf{u}^S, \bar{\mathbf{N}}^S), \quad (21b)$$

$$\frac{d\phi_0^c}{dx} = f^{S7}(\mathbf{u}^S, \bar{\mathbf{N}}^S). \quad (21c)$$

Then substituting these 7 higher order displacements together with Eq. (18) into Eq. (19) results in 8 differential equations, in which the right hand side only contains the terms of the equivalent resultant forces, $\bar{\mathbf{N}}^S = \{\bar{N}^{St}, \bar{N}^{Sb}, \bar{N}^{Sc}, \bar{M}^{Sb}, \bar{M}^{Sc}, \bar{V}^{St}, \bar{V}^{Sb}, \bar{V}^{Sc}\}$, and lower order displacements, $\mathbf{u}^S = \{u^{St}, u_0^{Sb}, u_0^{Sc}, w^{St}, w_0^{Sb}, w_0^{Sc}, w_{0,x}^{Sb}, \phi_0^{Sc}\}$. The are noted as,

$$\frac{d\bar{N}^{St}}{dx} = f^{S8}(\mathbf{u}_S, \bar{\mathbf{N}}^S); \quad \frac{d\bar{N}^{Sb}}{dx} = f^{S9}(\mathbf{u}_S, \bar{\mathbf{N}}^S); \quad \frac{d\bar{N}^{Sc}}{dx} = f^{S10}(\mathbf{u}_S, \bar{\mathbf{N}}^S), \quad (22a)$$

$$\frac{d\bar{M}^{Sb}}{dx} = f^{S11}(\mathbf{u}_S, \bar{\mathbf{N}}^S); \quad \frac{d\bar{M}^{Sc}}{dx} = f^{S12}(\mathbf{u}_S, \bar{\mathbf{N}}^S), \quad (22b)$$

$$\frac{d\bar{V}^{St}}{dx} = f^{S13}(\mathbf{u}_S, \bar{\mathbf{N}}^S); \quad \frac{d\bar{V}^{Sb}}{dx} = f^{S14}(\mathbf{u}_S, \bar{\mathbf{N}}^S); \quad \frac{d\bar{V}^{Sc}}{dx} = f^{S15}(\mathbf{u}_S, \bar{\mathbf{N}}^S), \quad (22c)$$

where $f^{Sj}(\mathbf{u}^S, \bar{\mathbf{N}}^S)$ ($j = 1, \dots, 15$) stand for the final expressions of the right-hand side, and are linear algebra expressions in terms of \mathbf{u}^S and $\bar{\mathbf{N}}^S$. These detailed expressions are long and thus are omitted for conciseness.

With the last equation for $w_{0,x}^{Sb}$,

$$\frac{dw_0^{Sb}}{dx} = w_{0,x}^{Sb}, \quad (22d)$$

there are 16 first order differential equations in terms of 16 unknowns. Eight of the unknowns are the equivalent resultant forces of the substrate part, $\bar{N}^{St,Sb,Sc}$, $\bar{M}^{Sb,Sc}$, $\bar{V}^{St,Sb,Sc}$, and other 8 unknowns are the lower order displacements, u^{St} , w^{St} , $u_0^{Sb,Sc}$, $w_0^{Sb,Sc}$, $w_{0,x}^{Sb}$, ϕ_0^{Sc} .

2.3.3 Governing equations of the debonded part

Same procedure is applied to the debonded part ($-a \leq x \leq 0$). The variation principle of Eq. (13) leads to 3 equations, and then considering the relation between the displacements and the resultant forces, one can obtain 6 first order differential equations, which are

$$\frac{d\bar{N}^{Dt}}{dx} = -p^t; \quad \frac{d\bar{V}^{Dt}}{dx} = -q^{st}, \quad (23a)$$

$$\frac{d\bar{M}^{Dt}}{dx} = \bar{V}^{Dt} - m^b; \quad \frac{du_0^{Dt}}{dx} = \frac{\bar{N}^{Dt}}{c_{11}^t f_t}, \quad (23b)$$

$$\frac{dw_{0,x}^{Dt}}{dx} = -12 \frac{\bar{M}^{Dt}}{c_{11}^t f_t^3}; \quad \frac{dw_0^{Dt}}{dx} = w_{0,x}^{Dt}, \quad (23c)$$

where \bar{N}^{Dt} , \bar{V}^{Dt} , and \bar{M}^{Dt} are the resultant axial force, shear force, and bending moment in the debonded part. \bar{N}^{Dt} and \bar{M}^{Dt} are defined as,

$$[\bar{N}^{Dt}, \bar{M}^{Dt}] = [N_x^{Dt}, M_y^{Dt}] = \int_c^{c+f_t} \left[1, \left(z - c - \frac{f_t}{2} \right) \right] \sigma_{xx}^{Dt} dz. \quad (24)$$

2.4 Boundary conditions at edges

At both edges, either displacements or external forces are prescribed, the boundary conditions of the left edge are: at $x = -a$,

$$\bar{N}^{St} = 0, \quad (25a)$$

$$\bar{V}^{St} = 0 , \quad (25b)$$

$$u_0^{Dt} = \tilde{u}_0^t \quad \text{or} \quad \bar{N}^{Dt} = \tilde{N}_{-a}^t , \quad (25c)$$

$$w_0^{Dt} = \tilde{w}_0^t \quad \text{or} \quad \bar{V}^{Dt} = \tilde{V}_{-a}^t , \quad (25d)$$

$$w_{0,x}^{Dt} = \tilde{w}_{0,x}^t \quad \text{or} \quad \bar{M}^{Dt} = \tilde{M}_{-a}^t , \quad (25e)$$

$$u_0^{Sc} = \tilde{u}_0^c \quad \text{or} \quad \bar{N}^{Sc} = \tilde{N}_{-a}^c , \quad (25f)$$

$$w_0^{Sc} = \tilde{w}_0^c \quad \text{or} \quad \bar{V}^{Sc} = \tilde{V}_{-a}^c , \quad (25g)$$

$$\phi_0^{Sc} = \tilde{\phi}_0^c \quad \text{or} \quad \bar{M}^{Sc} = \tilde{M}_{-a}^c , \quad (25h)$$

$$u_0^{Sb} = \tilde{u}_0^b \quad \text{or} \quad \bar{N}^{Sb} = \tilde{N}_{-a}^b , \quad (25i)$$

$$w_0^{Sb} = \tilde{w}_0^b \quad \text{or} \quad \bar{V}^{Sb} = \tilde{V}_{-a}^b , \quad (25j)$$

$$w_{0,x}^{Sb} = \tilde{w}_{0,x}^b \quad \text{or} \quad \bar{M}^{Sb} = \tilde{M}_{-a}^b . \quad (25k)$$

Similarly, boundary conditions of the right edge are: at $x = L$,

$$u_0^{Bt} = \tilde{u}_0^t \quad \text{or} \quad \bar{N}^{Bt} = \tilde{N}_L^t , \quad (26a)$$

$$w_0^{Bt} = \tilde{w}_0^t \quad \text{or} \quad \bar{V}^{Bt} = \tilde{V}_L^t , \quad (26b)$$

$$w_{0,x}^{Bt} = \tilde{w}_{0,x}^t \quad \text{or} \quad \bar{M}^{Bt} = \tilde{M}_L^t , \quad (26c)$$

$$u_0^{Bc} = \tilde{u}_0^c \quad \text{or} \quad \bar{N}^{Bc} = \tilde{N}_L^b , \quad (26d)$$

$$w_0^{Bc} = \tilde{w}_0^c \quad \text{or} \quad \bar{V}^{Bc} = \tilde{V}_L^c , \quad (26e)$$

$$\phi_0^{Bc} = \tilde{\phi}_0^c \quad \text{or} \quad \bar{M}^{Bc} = \tilde{M}_L^c , \quad (26f)$$

$$u_0^{Bb} = \tilde{u}_0^b \quad \text{or} \quad \bar{N}^{Bb} = \tilde{N}_L^b , \quad (26g)$$

$$w_0^{Bb} = \tilde{w}_0^b \quad \text{or} \quad \bar{V}^{Bb} = \tilde{V}_L^b , \quad (26h)$$

$$w_{0,x}^{Bb} = \tilde{w}_{0,x}^b \quad \text{or} \quad \bar{M}^{Bb} = \widetilde{M}_L^b . \quad (26i)$$

where the tilde over the symbol stands for the prescribed displacement or load.

2.5 Continuity conditions at debond tip section

At the cross section of $x = 0$, both displacement and force continuity conditions are required. The displacement continuity conditions are given directly, as:

$$u_0^{Dt}(0) = u_0^{Bt}(0) ; \quad w_0^{Dt}(0) = w_0^{Bt}(0) ; \quad w_{0,x}^{Dt}(0) = w_{0,x}^{Bt}(0) , \quad (27a)$$

$$u_0^{Sc}(0) = u_0^{Bt}(0) ; \quad w_0^{Sc}(0) = w_0^{Bc}(0) ; \quad \phi_0^{Sc}(0) = \phi_0^{Bc}(0) , \quad (27b)$$

$$u_0^{Sb}(0) = u_0^{Bb}(0) ; \quad w_0^{Sb}(0) = w_0^{Bb}(0) ; \quad w_{0,x}^{Sb}(0) = w_{0,x}^{Bb}(0) , \quad (27c)$$

$$u^{St}(0) = u_0^{Bt}(0) + \frac{f_t}{2} w_{0,x}^{Bt}(0) ; \quad w^{St}(0) = w_0^{Bt}(0) . \quad (27d)$$

The force continuity conditions are derived from the variational principle, Eq. (13).

They are, at $x = 0$:

$$\bar{N}^{St} + \bar{N}^{Dt} - \bar{N}^{Bt} = 0 ; \quad \bar{V}^{St} + \bar{V}^{Dt} - \bar{V}^{Bt} = 0 , \quad (28a)$$

$$\bar{N}^{St} \frac{f_t}{2} - \bar{M}^{Dt} + M^{Bt} = 0 , \quad (28b)$$

$$\bar{N}^{Sc} = \bar{N}^{Bc} ; \quad \bar{M}^{Sc} = \bar{M}^{Bc} ; \quad \bar{V}^{Sc} = \bar{V}^{Bc} , \quad (28c)$$

$$\bar{N}^{Sb} = \bar{N}^{Bb} ; \quad \bar{M}^{Sb} = \bar{M}^{Bb} ; \quad \bar{V}^{Sb} = \bar{V}^{Bb} ; , \quad (28d)$$

Therefore, there are 20 continuity conditions at the connected cross section among the debonded part, substrate part, and the base part.

3. Results and Discussion

The finite element analysis software ABAQUS [12] is used to get finite element solutions for verifications. The finite element model of sandwich panel is built with isoparametric 8-node biquadratic plane stress element (CPS8R). The mesh is refined at the debonded region and collapsed elements are used at the crack tip to include the singularity. A convergence study was carried out first and the finite element model is shown in Fig. 3. In Part II deals with the fracture parameters, in particular, the stress intensity factors. However, for an interfacial crack, ABAQUS can only calculate the stress intensity factors when the bi-materials are isotropic and linear elastic [12]. Thus, for verification purposes, several sandwich panels made with isotropic faces and core are studied as numerical examples. It should be noted, however, that the presented approach in this paper is also valid for interfacial debonds between orthotropic faces and cores.

3.1 Deformation of sandwich panels made with moderate core

To verify the high order model for the interfacial debonding, the deformed shape of a sandwich panel with a interfacial debond obtained from the EHSAPT approach is first compared with the one given by ABAQUS [12]. Consider a sandwich panel with a debond of length $a = 200$ mm existing between the top face and the core. The length of base part is $L = 300$ mm. Thus, the total length is $L + a = 500$ mm. It is made of Aluminum faces and Al foam core. The material properties are listed in Table 1. The thicknesses of the top, bottom, and core are $f_t = f_b = 2$ mm, and $2c = 20$ mm, respectively. Figs. 4a,b give the deformed shape when the right edge ($x = L$) is clamped, and shear forces and bending moments are applied at the left edge ($x = -a$), namely, $\tilde{Q}^t = -0.5$ N, $\tilde{Q}^b = 0.5$ N, $\tilde{M}^t = -100$ Nmm, and $\tilde{M}^b = 100$ Nmm. Fig. 4a shows the deformed shape given by ABAQUS, in which 20683 CPS8R elements are used to build the finite element model

and collapsed elements are used at the crack tip to include the singularity. Fig. 4b is the deformed shape given by the EHSAPT after solving the governing equations, Eqs (15-17) and (21-23), simultaneously. These two are identical to each other. When the same loads are applied to both the debonded part and the substrate part, the debonded face experiences much larger deformation since the bending stiffness of the substrate part is much larger.

The comparison between the debonded surfaces at the crack tip given by ABAQUS and the one by EHSAPT is shown in Fig. 4c. In Fig. 4c, the blue solid lines are the boundary lines of the debonded part, substrate part, and base part given by the EHSAPT. The blue dash lines are the intersection between the base part and the debonded part, and between the base part and the substrate part. The red dots are final location of the debonded surface given by ABAQUS.

It is seen that the displacement field given by the EHSAPT agrees well with the one given by ABAQUS, even at the crack tip region. Fig. 4c also shows that the displacement continuity of the faces and core at the intersection between the base part and the debonded part, and at the intersection between the base part and the substrate part are satisfied.

Table 2 lists the tip displacements of the debonded part and the substrate part. Various loading conditions are considered, including in-plane axial forces only, shear force only, bending moment only, and various combinations of axial force, shear force and bending moment applied at the debonded edge. Both the axial displacement component, u , and transverse displacement component, w , obtained by the high-order approach (“EHSAPT”) are compared with the ones given by ABAQUS. Great agreement between the EHSAPT and the finite element results (ABAQUS) is observed. As expected, for the considered loads, sandwich panels with an interfacial debond experience more significant transverse

deformation than axial deformation. For the transverse displacement at the debonded edge, the relative difference between EHSAPT and ABAQUS is less than 2%. The lowest relative different is only 0.073% when $\tilde{N}^t = -\tilde{N}^b = 100$ N. The relative difference in the axial displacement between EHSAPT and ABAQUS is larger than then the relative difference of the transverse displacement. Considering the fact of that the magnitude of u is very small, the absolute difference of the axial displacement between EHSAPT and ABAQUS is quite small. Therefore, the EHSAPT approach can actually predict the deformation of a sandwich panel with a moderate core and an interfacial debond. The EHSAPT approach can easily handle the shear force and the shear deformation in the core.

3.2 Deformation of sandwich panels made with soft core

In this example, we consider a sandwich panel made with soft core. It is made of Aluminum faces and H100 core. The material properties are listed in Table 1. The ratio of the Young's modulus of the face sheets and the core sheet is $E_1^f/E_1^c \approx 538$. Same geometries and boundary conditions are considered, i.e., $f_t = f_b = 2$ mm, and $2c = 20$ mm, $a = 200$ mm and $L = 300$ mm. Table 3 gives the tip displacements of the debonded part and the substrate part when subjected various loads. When use soft H100 form as the core material, the deformation of the debonded part increase slightly. The transverse displacement is increased around 10%, and the change is mainly due to the deformation of the base part. The deformation of the substrate part may increase significantly, which depends on the loading condition. When only axial force is applied, using H100 soft core will only increase the transverse deformation of the substrate part around 10%. However, when shear forces or/and bending moments are applied at the debonded edge, using H100 soft core can increase the transverse deformation significantly, around 2500% for all other

four loading cases. The agreement between EHSAPT and ABAQUS is very good for the softer H100 core, as shown in Table 3. Thus, the EHSAPT approach can actually predict the deformation of a sandwich panel with a soft core and an interfacial debond.

3.3 Effects of various debond lengths

In order to examine the effect of crack length, Table 4 shows the results for sandwich panels with shorter debond length. The geometry and materials are the same as for Table 2. The total specimen length remains $L + a = 500$ mm. Two debond lengths, namely, $a = 100$ mm (half of the debond length in Tables 2-3), and $a = 20$ mm (one tenth of the debond length in Tables 2-3), are considered. Again, a good agreement is observed for sandwich panels with smaller debond lengths. Comparing Table 2 and Table 4, when the same forces are applied at the debonded edge, the deformation decreases as the debond length decreases.

The deformation obtained by EHSAPT agrees with the ones given by the finite element analysis. For the debonded top face, the relative difference in the axial displacement is smaller than 10%, and the relative difference in the transverse displacement is smaller than 7%. For the substrate part, due to the short length and higher bending stiffness , the deformation is very small, and thus the relative difference is higher than that of the debonded part. But again, the absolute difference is very small. Although shorter debond length results into a larger difference in the predicted displacements between EHSAPT and finite element analysis, the discrepancy in displacements does not affect the accuracy of the energy release and mode mixity prediction, as the energy release rate and mode mixity predicted by EHSAPT are given by the equivalent forces together with the displacement variables. The accuracy of predicted energy release rate and mode mixity by EHSAPT remains very high for shorted debond length, which will be discussed in detail in the Part II of this two-part

series of papers. The EHSAPT approach is also capable of modeling sandwich panels with short debond length.

4. Conclusions

A high order theory based on the Extended High Order Sandwich Panel Theory (EHSAPT) is developed to model sandwich panels with face/core interfacial debonds. A sandwich panel with an interfacial debond is divided into three parts, namely, the debonded face, substrate part, and the base part. The EHSAPT, which assumes the face/core should be perfectly bonded, is re-formulated through proposed high order displacement assumptions for the substrate part, which includes only the core and the bottom face. The proposed displacement fields of the substrate part are compatible with the ones from the existing EHSAPT, which is used to model the base part, which consists of both perfectly bonded faces and the core. The presented model ensures both traction and displacement continuity conditions at the common cross section of these parts. The high order shear deformation of the core, as well as its axial rigidity, and compressibility are all included in the formulation. By introducing concepts of equivalent resultant forces and moments, the governing equations are derived as sets of first order differential equations. Comparisons with finite element results show that the present approach can accurately predict the displacement field. Sandwich panels made with a wide range of material combinations are studied in the present work. The study includes sandwich panels made with moderate core - Aluminum foam core, and the ones made with soft core - H100 core. The presented approach shows high accuracy and can handle the shear force easily. The analysis is comprehensive and is done for a general asymmetric sandwich construction. The presented model is suitable for sandwich panels made with a wide range of core materials, including very soft cores and with non-isotropic

faces and core. It applies to sandwich panels subjected to various boundary conditions and loading conditions, such as the Single Cantilever Beam (SCB) sandwich composite specimen, the Double Cantilever Beam (DCB) sandwich composite specimen, etc. Additionally, the present model is not limited to sandwich panels with one face/core interfacial debond located at the edge. By simply connecting multiple substrate parts, debonded parts and base parts, the present approach can be used to model sandwich panels with multiple face/core debonds and debonds located at the inside (not edge) of sandwich panels. Therefore, the present approach can serve as a general platform for the analysis of interfacial debonds of sandwich panels and evaluating corresponding fracture parameters.

Acknowledgments. The financial support of the Office of Naval Research, Grant N00014-20-1-2605, and the interest and encouragement of the Grant Monitors, Dr. Jessica Dibelka, Dr. Paul Hess and Dr. Y.D.S. Rajapakse, are both gratefully acknowledged. Z.Y. would also like to acknowledge the financial support through Worcester Polytechnic Institute startup funds.

References

- [1] Carlsson, L., and Kardomateas, G., 2011. *Structural and Failure Mechanics of Sandwich Composites*. Springer, New York.
- [2] Phan, C. N., Frostig, Y., and Kardomateas, G. A., 2012. “Analysis of sandwich beams with a compliant core and with in-plane rigidity-extended high-order sandwich panel theory versus elasticity”. *Journal of Applied Mechanics*, 79(4), pp. 041001-041011.
- [3] Yuan, Z., Kardomateas, G. A., and Frostig, Y., 2015. “Finite element formulation based on the extended high-order sandwich panel theory”. *AIAA Journal*, 53(10), pp.

3006-3015.

- [4] Frostig, Y., Baruch, M., Vilnay, O., and Sheinman, I., 1992. "High-order theory for sandwich-beam behavior with transversely flexible core". *Journal of Engineering Mechanics*, 118(5), pp. 1026-1043.
- [5] Phan, C.N., Kardomateas, G.A. and Frostig, Y, "Blast Response of a Sandwich Beam/Wide Plate based on the Extended High-Order Sandwich Panel Theory (EHSAPT) and Comparison with Elasticity", *Journal of Applied Mechanics* (ASME), vol. 80, 061005 (11pages) November 2013, doi: 10.1115/1.4023619.
- [6] Yuan, Z., and Kardomateas, G. A., 2018. "Nonlinear dynamic response of sandwich wide panels". *International Journal of Solids and Structures*, 148-149, pp. 110-121.
- [7] Phan, C.N., Karomateas, G.A. and Frostig, Y., "Global Buckling of a Sandwich Wide Panel/Beam based on the Extended High Order Theory", *AIAA Journal*, vol. 50, no. 8, pp. 1707-1716, Aug 2012, DOI: 10.2514/1.J051454.
- [8] Phan, C.N., Bailey, N.W., Kardomateas, G.A. and Battley, M.A., "Wrinkling of Sandwich Wide Panels/Beams based on the Extended High Order Sandwich Panel Theory: Formulation, Comparison with Elasticity and Experiments", *Archive of Applied Mechanics* (special Issue in Honor of Prof. Anthony Kounadis), vol. 82, issue 10-11, pp. 1585-1599, October 2012.
- [9] Yuan, Z., and Kardomateas, G. A., 2018. "Nonlinear stability analysis of sandwich wide panels-part I: Buckling behavior". *Journal of Applied Mechanics*, 85(8), p. 081006.
- [10] Yuan, Z., and Kardomateas, G. A., 2018. "Nonlinear stability analysis of sandwich wide panels-part II: Postbuckling response". *Journal of Applied Mechanics*, 85(8), p.

081007.

[11] Yuan, Z., Kardomateas, G. A., and Frostig, Y., 2016. “Geometric nonlinearity effects in the response of sandwich wide panels”. *Journal of Applied Mechanics*, 83(9), pp. 091008-1 to 091008-10.

[12] Dassault Systemes Simulia Corp. SIMULIA User Assistance 2018. Providence, RI.

Table 1. Material properties

Isotropic, $G = E/[2(1 + \nu)]$		
Aluminum face	Aluminum foam core	H100 core
$E = 70,000$ MPa	$E = 7,000$ MPa	$E = 130$ MPa
$\nu = 0.30$	$\nu = 0.32$	$\nu = 0.30$

Table 2. Tip displacements - Aluminum faces and Aluminum foam core*

\tilde{N}^t	\tilde{N}^b	\tilde{V}^t	\tilde{V}^b	\tilde{M}^t	\tilde{M}^b	Debonded part, $x = -a, z = c + f_t/2$, (mm)		Substrate part, $x = -a, z = c$, (mm)					
						EHSAPT	ABAQUS	EHSAPT	ABAQUS				
u	w	u	w	u	w	u	w	u	w				
100	-100	0	0	0	0	-0.3310	-6.0174	-0.3312	-6.0107	-0.2251	-6.7988	-0.2243	-6.7938
0	0	-0.5	0.5	0	0	6.169E-04	29.3298	6.597E-04	29.6754	-0.0139	-0.1259	-0.0141	-0.1287
0	0	0	0	-100	100	6.128E-04	43.6117	6.524E-04	43.6526	-0.0243	-0.1761	-0.0247	-0.1776
100	-100	0	0	-100	100	-0.3304	37.5943	-0.3305	37.9419	-0.2494	-6.9749	-0.2490	-6.9714
0	0	-0.5	0.5	-100	100	1.230E-03	72.9415	1.312E-03	73.6280	-0.0382	-0.3020	-0.0388	-0.3063

*Results for debond length of 200 mm and total length of 500 mm

Table 3. Tip displacements - Aluminum faces and H100 foam core*

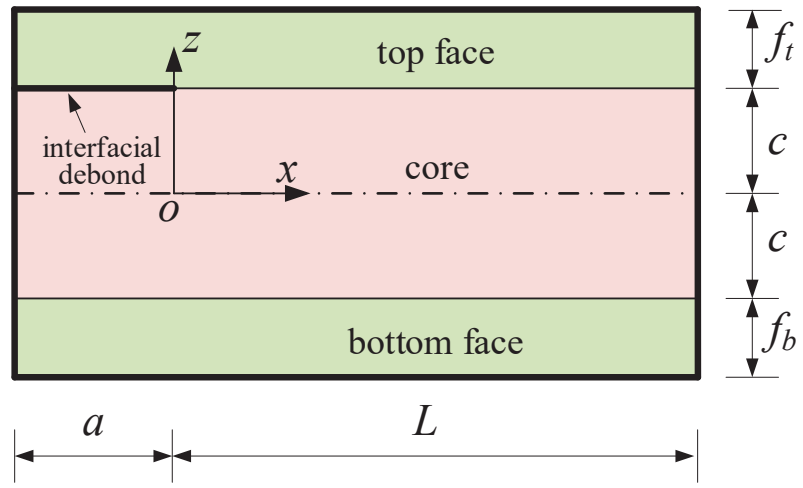
Loads at $x = -a$ (N or Nmm)						Debonded part, $x = -a, z = c + f_t/2$, (mm)		Substrate part, $x = -a, z = c$, (mm)			
						EHSAPT		ABAQUS		EHSAPT	
\tilde{N}^t	\tilde{N}^b	\tilde{V}^t	\tilde{V}^b	\tilde{M}^t	\tilde{M}^b	u	w	u	w	u	w
100	-100	0	0	0	0	-0.3560	-6.6611	-0.3561	-6.6503	-0.2384	-7.6660
0	0	-0.5	0.5	0	0	-1.192E-04	32.7974	-1.0239E-04	33.1444	-0.4952	-3.2822
0	0	0	0	-100	100	-1.202E-04	47.0181	-1.0436E-04	47.3481	-0.9148	-4.7692
100	-100	0	0	-100	100	-0.3561	40.3570	-0.3562	40.6978	-1.1532	-12.4352
0	0	-0.5	0.5	-100	100	-2.394E-04	79.8155	-2.0674E-04	80.4925	-1.4100	-8.0514

*Results for debond length of 200 mm and total length of 500 mm

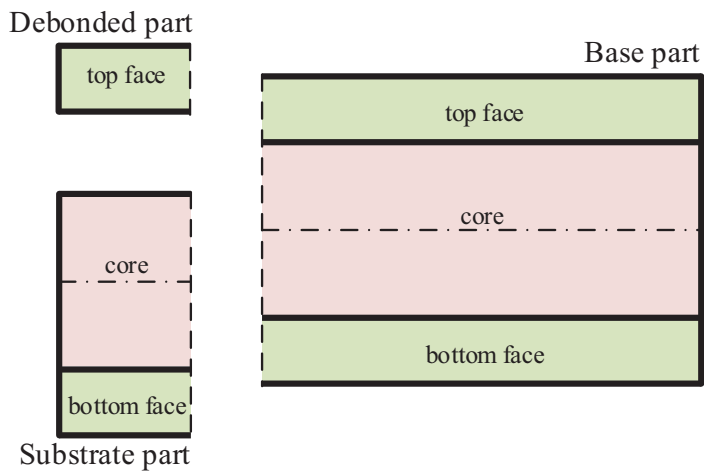
Table 4. Tip displacements for various debond lengths - Aluminum faces and Aluminum foam core*

Loads at $x = -a$ (N or Nmm)				Debonded part, $x = -a, z = c + f_t/2$, (mm)				Substrate part, $x = -a, z = c$, (mm)			
				EHSAPT		ABAQUS		EHSAPT		ABAQUS	
\tilde{V}^t	\tilde{V}^b	\tilde{M}^t	\tilde{M}^b	u	w	u	w	u	w	u	w
$a = 100$ mm											
-0.5	0.5	0	0	3.105E-04	3.7633	3.335E-04	3.8516	-4.004E-03	-1.896E-02	-4.119E-03	-1.974E-02
0	0	-100	100	6.128E-04	11.0940	6.524E-04	11.2656	-1.256E-02	-5.030E-02	-1.295E-02	-5.045E-02
-0.5	0.5	-100	100	9.234E-04	14.8572	9.859E-04	15.1172	-1.657E-02	-6.927E-02	-1.707E-02	-7.020E-02
$a = 20$ mm											
-0.5	0.5	0	0	6.560E-05	0.0370	7.265E-05	0.0412	-3.286E-04	-3.968E-04	-3.532E-04	-4.346E-04
0	0	-100	100	6.078E-04	0.5081	6.447E-04	0.5447	-3.270E-03	-4.340E-03	-3.617E-03	-3.412E-03
-0.5	0.5	-100	100	6.734E-04	0.5451	7.173E-04	0.5858	-3.598E-03	-4.736E-03	-3.970E-03	-3.847E-03

*Total length of 500 mm



(a)



(b)

Figure 1: Sketch of a sandwich panel with a face/core interfacial debond: (a) definition of the face/core debond configuration, (b) definition of the debonded, substrate and base parts

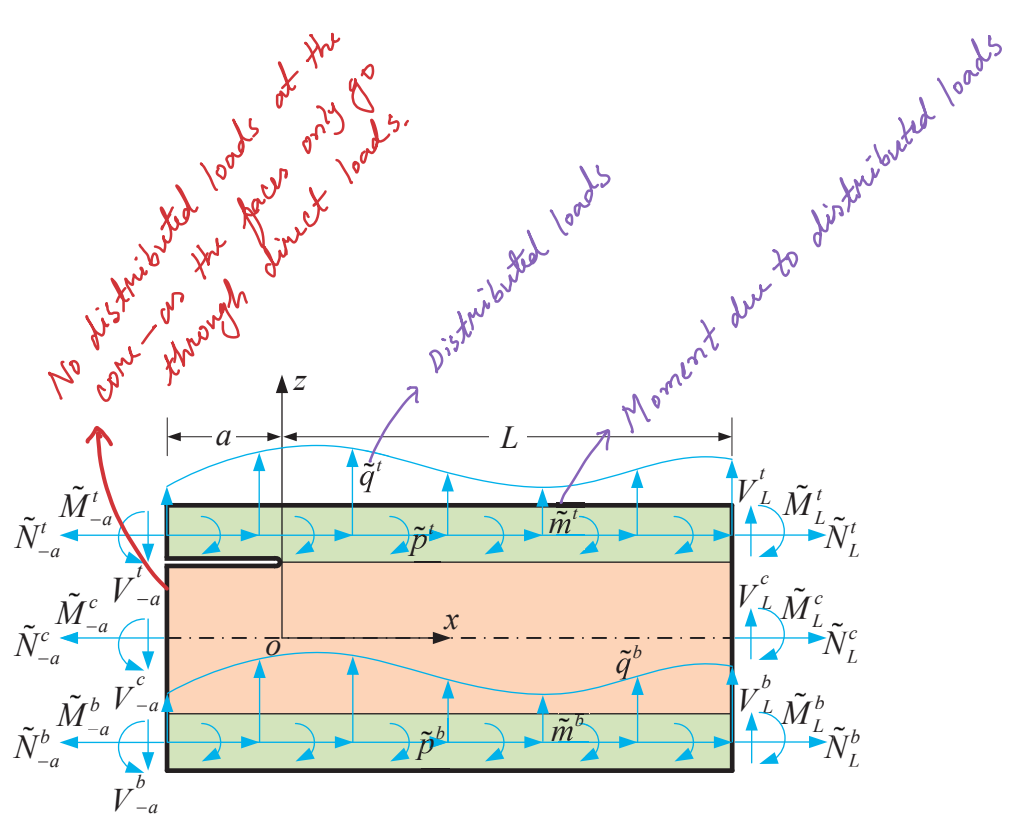


Figure 2: Externally applied loads

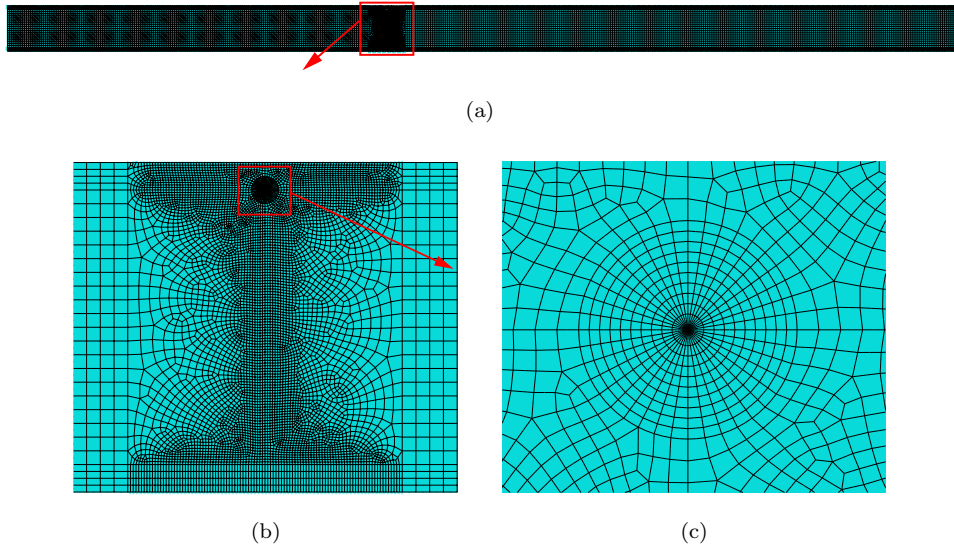


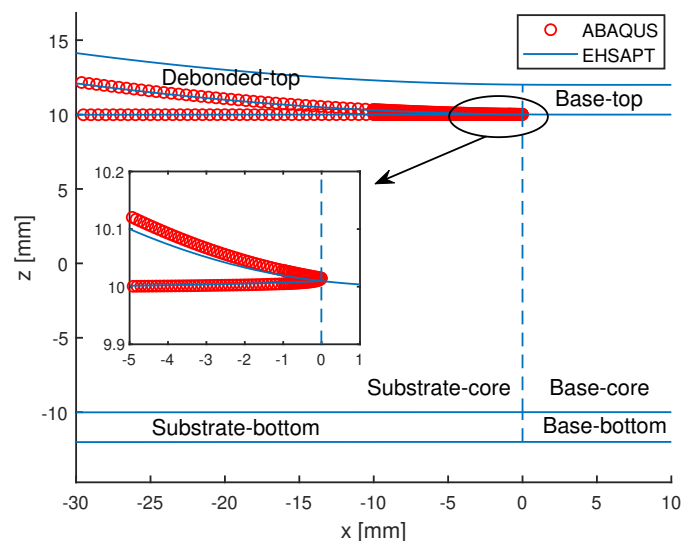
Figure 3: Finite element model of a sandwich panel with an interfacial debond in ABAQUS ($f_t = f_b = 2\text{mm}$, $2c = 20 \text{ mm}$, $L = 300\text{mm}$, and $a = 200 \text{ mm}$): (a), whole beam; (b), middle part of the FE model; (c) finite element model for the debond tip



(a)



(b)



(c)

Figure 4: Deformed shape of a sandwich panel with a face/core interfacial debond:
 (a)ABAQUS; (b)EHSAPT; (c)Comparison between ABAQUS and EHSAPT at debonded
 region